

Combined Target-Based and Ligand-Based Drug Design Approach as a Tool To Define a Novel 3D-Pharmacophore Model of Human A₃ Adenosine Receptor Antagonists: Pyrazolo[4,3-*e*]1,2,4-triazolo[1,5-*c*]pyrimidine Derivatives as a Key Study

Stefano Moro,^{*,†} Paolo Braiuca,[‡] Francesca Deflorian,[†] Cristina Ferrari,[†] Giorgia Pastorin,[‡] Barbara Cacciari,[§] Pier Giovanni Baraldi,[§] Katia Varani,^{||} Pier Andrea Borea,^{||} and Giampiero Spalluto^{*,‡}

Molecular Modeling Section, Dipartimento di Scienze Farmaceutiche, Università di Padova, Via Marzolo 5, I-35131 Padova, Italy, Dipartimento di Scienze Farmaceutiche, Università degli Studi di Trieste, Piazzale Europa 1, I-34127 Trieste, Italy, Dipartimento di Scienze Farmaceutiche, Università degli Studi di Ferrara, Via Fossato di Mortara 17-19, I-44100 Ferrara, Italy, and Dipartimento di Medicina Clinica e Sperimentale-Sezione di Farmacologia, Università degli Studi di Ferrara, Via Fossato di Mortara 17-19, I-44100 Ferrara, Italy

Received May 5, 2004

A combined target-based and ligand-based drug design approach has been carried out to define a novel pharmacophore model of the human A₃ receptor antagonists. High throughput molecular docking and comparative molecular field analysis (CoMFA) have been used in tandem to assemble a new target based pharmacophore model. In parallel, to provide more accurate information about the putative binding site of these A₃ inhibitors, a rhodopsin-based model of the human A₃ receptor was built and a novel Y-shape binding motif has been proposed. Docking-based structure superimposition has been used to perform a quantitative study of the structure–activity relationships for binding of these pyrazolo–triazolo–pyrimidines to adenosine A₃ receptor using CoMFA. Both steric and the electrostatic contour plots obtained from the CoMFA analysis nicely fit on the hypothetical binding site obtained by molecular docking. On the basis of the combined hypothesis, we have designed, synthesized, and tested 17 new derivatives. Consistently, the predicted K_i values were very close to the experimental values.

Introduction

Many physiological functions may be regulated by interaction of adenosine with a set of specific receptors, classified as A₁, A_{2A}, A_{2B}, and A₃.¹ For this reason, adenosine receptors could be considered in the treatment of different pathophysiological conditions.^{2–6} Adenosine receptor subtypes belong to the family of seven transmembrane domain receptor coupled G proteins, and they exert their physiological role by activation or inhibition of different second messenger systems.^{2–6}

A₃ adenosine receptors are associated with cerebroprotection^{7,8} and cardioprotection⁹ effects of adenosine agonists and effects on the immune and inflammatory systems.^{3,10} The A₃ adenosine receptor subtype, recently cloned from different species (e.g. rat, human, dog, sheep),^{11,12} is coupled to the modulation of at least two second messenger systems: inhibition of adenylate cyclase and stimulation of phospholipase C and D.^{11,12} In human, A₃ receptors have been found in several organs, such as lung, liver, kidney, and heart, and with a lower density in brain.^{9,11,12} This receptor subtype is under examination in relation to its potential thera-

peutic applications. In particular, antagonists for A₃ receptors seem to be useful for the treatment of inflammation and regulation of cell growth.^{2,13} However, concerning specifically the potential treatment of inflammation, the role of both A₃ agonists and antagonists is still ambiguous.³

In the last five years, many efforts have been conducted searching potent and selective human A₃ adenosine antagonists. In this field several different classes of compounds, possessing good affinity (nM range) and with a broad range of selectivity, have been proposed.^{10,14,15}

Recently, our group has synthesized a new series of pyrazolo–triazolo–pyrimidines bearing different substitutions at the N⁵ and N⁸ positions which have been described as highly potent and selective human A₃ adenosine receptor antagonists. Table 1 summarizes all the compounds (**1–106**) previously synthesized as human A₃ adenosine receptor antagonists.^{15–20}

A combined target-based and ligand-based drug design approach has been carried out to define a novel pharmacophore model of the human A₃ receptor antagonists. High throughput molecular docking and comparative molecular field analysis (CoMFA) have been used in tandem to assemble a novel target-based pharmacophore model. In parallel, to provide more accurate information about the putative binding site of these A₃ inhibitors, a rhodopsin-based model of the human A₃ receptor was built, and more than 100 pyrazolotriazolopyrimidine ligands were docked into the putative ligand binding site. A novel Y-shaped binding

* Author to whom correspondence should be addressed. Mailing address: Molecular Modeling Section, Department of Pharmaceutical Sciences, University of Padova, Via Marzolo 5, I-35131 Padova, Italy. Tel: +39 049 8275704. Fax: +39 049 827 5366. E-mail: stefano.moro@unipd.it.

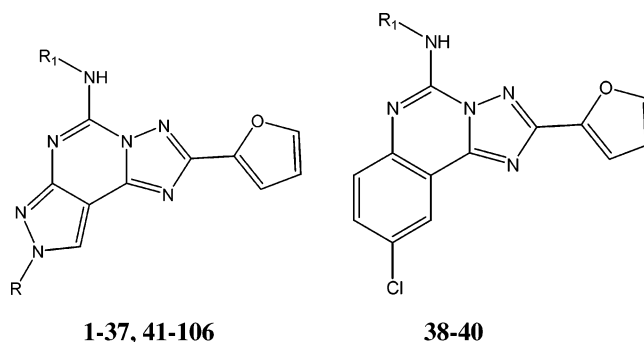
† Università di Padova.

‡ Università degli Studi di Trieste.

§ Dipartimento di Scienze Farmaceutiche, Università degli Studi di Ferrara.

|| Dipartimento di Medicina Clinica e Sperimentale-Sezione di Farmacologia, Università degli Studi di Ferrara.

Table 1. Structures and Human A₃ Binding Affinities for All Analyzed Compounds



no.	R	R ¹	hA ₃ K _i (nM)	no.	R	R ¹	hA ₃ K _i (nM)
1	H	H	348 (267–453)	56	C ₂ H ₅	4-NO ₂ -Ph-NHCO	0.65 (0.56–0.75)
2	H	4-MeO-Ph-NHCO	0.14 (0.08–0.27)	57	C ₂ H ₅	4-CH ₃ -Ph-NHCO	0.14 (0.11–0.18)
3	H	3-Cl-Ph-NHCO	0.50 (0.34–0.73)	58	C ₂ H ₅	4-Br-Ph-NHCO	0.37 (0.29–0.47)
4	CH ₃	H	300 (265–339)	59	C ₂ H ₅	4-F-Ph-NHCO	0.86 (0.77–0.97)
5	CH ₃	4-MeO-Ph-NHCO	0.20 (0.17–0.24)	60	C ₂ H ₅	4-CF ₃ -Ph-NHCO	0.97 (0.86–1.09)
6	CH ₃	3-Cl-Ph-NHCO	0.40 (0.24–0.64)	61	C ₂ H ₅	2-OMe-Ph-NHCO	0.56 (0.49–0.64)
7	C ₂ H ₅	H	331 (285–385)	62	C ₂ H ₅	3-OMe-Ph-NHCO	0.86 (0.77–0.96)
8	C ₂ H ₅	4-MeO-Ph-NHCO	0.60 (0.51–0.70)	63	C ₂ H ₅	2-Cl-Ph-NHCO	0.30 (0.23–0.40)
9	C ₂ H ₅	3-Cl-Ph-NHCO	1.60 (1.42–1.79)	64	C ₂ H ₅	4-Cl-Ph-NHCO	0.20 (0.15–0.28)
10	<i>n</i> -C ₃ H ₇	H	408 (364–460)	65	<i>n</i> -C ₃ H ₇ ^a	Ph-NHCO	0.15 (0.10–0.18)
11	<i>n</i> -C ₃ H ₇	4-MeO-Ph-NHCO	0.80 (0.63–0.1.00)	66	<i>n</i> -C ₃ H ₇	3,4-Cl ₂ -Ph-NHCO	2.5 (2.0–3.1)
12	<i>n</i> -C ₃ H ₇	3-Cl-Ph-NHCO	0.91 (0.85–0.98)	67	<i>n</i> -C ₃ H ₇	3,4-O-CH ₂ O- -Ph-NHCO	0.30 (0.22–0.40)
13	CH ₂ CH=CH ₂	4-MeO-Ph-NHCO	0.48 (0.32–0.74)	68	<i>n</i> -C ₃ H ₇	4-NO ₂ -Ph-NHCO	0.81 (0.63–1.04)
14	<i>n</i> -C ₄ H ₉	H	600 (525–691)	69	<i>n</i> -C ₃ H ₇	4-CH ₃ -Ph-NHCO	0.40 (0.31–0.50)
15	<i>n</i> -C ₄ H ₉	4-MeO-Ph-NHCO	0.32 (0.27–0.34)	70	<i>n</i> -C ₃ H ₇	4-Br-Ph-NHCO	0.45 (0.37–0.56)
16	<i>n</i> -C ₄ H ₉	3-Cl-Ph-NHCO	0.60 (0.52–0.68)	71	<i>n</i> -C ₃ H ₇	4-F-Ph-NHCO	0.29 (0.21–0.40)
17	<i>t</i> -C ₄ H ₉	H	1149 (1061–1245)	72	<i>n</i> -C ₃ H ₇	4-CF ₃ -Ph-NHCO	0.51 (0.42–0.62)
18	<i>t</i> -C ₄ H ₉	4-MeO-Ph-NHCO	0.80 (0.63–1.00)	73	<i>n</i> -C ₃ H ₇	2-OMe-Ph-NHCO	0.34 (0.27–0.43)
19	<i>t</i> -C ₄ H ₉	3-Cl-Ph-NHCO	2.78 (2.13–3.62)	74	<i>n</i> -C ₃ H ₇	3-OMe-Ph-NHCO	0.40 (0.32–0.50)
20	(CH ₃) ₂ CHCH ₂ CH ₂	H	700 (664–738)	75	<i>n</i> -C ₃ H ₇	2-Cl-Ph-NHCO	0.71 (0.61–0.83)
21	(CH ₃) ₂ CHCH ₂ CH ₂	4-MeO-Ph-NHCO	30 (23–40)	76	<i>n</i> -C ₃ H ₇	4-Cl-Ph-NHCO	0.34 (0.24–0.48)
22	(CH ₃) ₂ CHCH ₂ CH ₂	3-Cl-Ph-NHCO	40 (33–48)	77	<i>n</i> -C ₃ H ₇ ^a	Ph-NHCO	0.21 (0.12–0.37)
23	(CH ₃) ₂ C=CHCH ₂	H	811 (691–952)	78	<i>n</i> -C ₄ H ₉	3,4-Cl ₂ -Ph-NHCO	3.7 (3.2–4.3)
24	(CH ₃) ₂ C=CHCH ₂	4-MeO-Ph-NHCO	40 (35–47)	79	<i>n</i> -C ₄ H ₉	3,4-O-CH ₂ O- -Ph-NHCO	0.50 (0.40–0.62)
25	(CH ₃) ₂ C=CHCH ₂	3-Cl-Ph-NHCO	55 (50–61)	80	<i>n</i> -C ₄ H ₉	4-NO ₂ -Ph-NHCO	0.55 (0.46–0.64)
26	PhCH ₂ CH ₂	H	280 (347–317)	81	<i>n</i> -C ₄ H ₉	4-CH ₃ -Ph-NHCO	0.21 (0.16–0.28)
27	PhCH ₂ CH ₂	4-MeO-Ph-NHCO	0.98 (1.22–1.78)	82	<i>n</i> -C ₄ H ₉	4-Br-Ph-NHCO	0.91 (0.82–1.02)
28	PhCH ₂ CH ₂	3-Cl-Ph-NHCO	8.0 (7.2–8.9)	83	<i>n</i> -C ₄ H ₉	4-F-Ph-NHCO	0.80 (0.70–0.92)
29	PhCH ₂ CH ₂ CH ₂	H	430 (378–488)	84	<i>n</i> -C ₄ H ₉	4-CF ₃ -Ph-NHCO	0.72 (0.61–0.84)
30	PhCH ₂ CH ₂ CH ₂	4-MeO-Ph-NHCO	40 (33–48)	85	<i>n</i> -C ₄ H ₉	2-OMe-Ph-NHCO	0.57 (0.46–0.70)
31	PhCH ₂ CH ₂ CH ₂	3-Cl-Ph-NHCO	60 (51–70)	86	<i>n</i> -C ₄ H ₉	3-OMe-Ph-NHCO	0.60 (0.53–0.68)
32	2,4,5-Br ₃ -Ph-CH ₂ CH ₂	H	4481 (3650–5501)	87	<i>n</i> -C ₄ H ₉	2-Cl-Ph-NHCO	0.86 (0.76–0.98)
33	2,4,5-Br ₃ -Ph-CH ₂ CH ₂	4-MeO-Ph-NHCO	25 (17–36)	88	<i>n</i> -C ₄ H ₉	4-Cl-Ph-NHCO	0.43 (0.37–0.50)
34	2,4,5-Br ₃ -Ph-CH ₂ CH ₂	3-Cl-Ph-NHCO	71 (65–78)	89	CH ₃	Ph-CH ₂ CO	0.81 (0.69–0.97)
35	2-(α -naphthyl)ethyl	H	3416 (3228–3614)	90	C ₂ H ₅	Ph-CH ₂ CO	1.03 (0.79–1.34)
36	2-(α -naphthyl)ethyl	4-MeO-Ph-NHCO	16 (14–19)	91	<i>n</i> -C ₃ H ₇	Ph-CH ₂ CO	1.01 (0.65–1.58)
37	2-(α -naphthyl)ethyl	3-Cl-Ph-NHCO	51 (34–76)	92	<i>n</i> -C ₄ H ₉	Ph-CH ₂ CO	1.11 (0.74–1.67)
38 ^a		H	85 (76–95)	93	PhCH ₂ CH ₂	CONHCH(CH ₃) ₂	(7.3–11) 9.0
39		4-MeO-Ph-NHCO	0.14 (0.08–0.24)	94	PhCH ₂ CH ₂	CONHC(CH ₃) ₃	4.9 (3.4–7.2)
40		3-Cl-Ph-NHCO	0.19 (0.13–0.27)	95	(CH ₃) ₂ CHCH ₂ CH ₂	CONHCH(CH ₃) ₂	65 (56–75)
41	CH ₃	Ph-NHCO	0.16 (0.13–0.20)	96	(CH ₃) ₂ CHCH ₂ CH ₂	CONHC(CH ₃) ₃	39 (24–63)
42	CH ₃	3,4-Cl ₂ -Ph-NHCO	3.40 (3.05–3.78)	97	CH ₃ CH ₂ CH ₂	CONHCH(CH ₃) ₂	21 (15–28)
43	CH ₃	3,4-O-CH ₂ O- -Ph-NHCO	0.24 (0.21–0.28)	98	CH ₃ CH ₂ CH ₂	CONHC(CH ₃) ₃	15 (10–21)
44	CH ₃	4-NO ₂ -Ph-NHCO	0.43 (0.38–0.48)	99	PhCH ₂ CH ₂ CH ₂	CONHCH(CH ₃) ₂	55 (46–65)
45	CH ₃	4-CH ₃ -Ph-NHCO	0.31 (0.25–0.38)	100	PhCH ₂ CH ₂ CH ₂	CONHC(CH ₃) ₃	65 (56–75)
46	CH ₃	4-Br-Ph-NHCO	0.46 (0.39–0.54)	101	PhCH ₂ CH ₂	CO(CH ₂) ₃ NH ₃ ⁺ Cl ⁻	65 (42–103)
47	CH ₃	4-F-Ph-NHCO	0.34 (0.28–0.41)	102	PhCH ₂ CH ₂	CO(CH ₂) ₃ NH-COOC(CH ₃) ₃	1480 (1019–2149)
48	CH ₃	4-CF ₃ -Ph-NHCO	0.74 (0.64–0.86)	103	(CH ₃) ₂ CHCH ₂ CH ₂	CO(CH ₂) ₃ -NH ₃ ⁺ Cl ⁻	90 (73–110)
49	CH ₃	2-OMe-Ph-NHCO	0.70 (0.59–0.83)	104	(CH ₃) ₂ CHCH ₂ CH ₂	CO(CH ₂) ₃ NH-COOC(CH ₃) ₃	2488 (1993–3108)
50	CH ₃	3-OMe-Ph-NHCO	0.80 (0.71–0.91)	105	PhCH ₂ CH ₂	COCH ₂ NH ₃ ⁺ Cl ⁻	163 (137–193)
51	CH ₃	2-Cl-Ph-NHCO	0.91 (0.82–1.01)	106	PhCH ₂ CH ₂	CO(CH ₂) ₂ NH ₃ ⁺ Cl ⁻	80 (63–100)
52	CH ₃	4-Cl-Ph-NHCO	0.29 (0.23–0.36)				
53	C ₂ H ₅	Ph-NHCO	0.18 (0.13–0.23)				
54	C ₂ H ₅	3,4-Cl ₂ -Ph-NHCO	3.0 (2.7–3.4)				
55	C ₂ H ₅	3,4-O-CH ₂ O- -Ph-NHCO	0.27 (0.22–0.34)				

^a CGS15943.

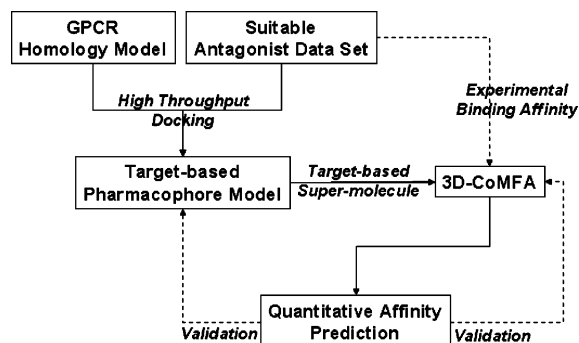


Figure 1. Flowchart describing our combined target-based and ligand-based drug design approach.

motif has been proposed for this class of A₃ inhibitors. Docking-based structure superimposition has been used to perform a quantitative study of structure–activity relationships using CoMFA. A remarkable correlation coefficient (cross-validated r^2_{cv}) of 0.840 was obtained. Both steric and electrostatic contour plots, obtained from the CoMFA analysis, nicely fit on the hypothetical binding site achieved by molecular docking. Following our computational approach, we have designed, synthesized, and tested 17 new derivatives. Consistently, the predicted K_i values were very close to the experimental values.

Results and Discussion

Our computational strategy has been summarized in Figure 1. We decided to combine a target-based approach (high throughput docking) and a quantitative ligand-based methodology like CoMFA to improve our capability to design new potent and selective human A₃ antagonists.

Starting from our recent rhodopsin-based model of the “resting state” of human A₃ receptor, we decide to perform high throughput docking to analyze the hypothetical binding conformation of more than 100 pyrazolotriazolopyrimidines recently synthesized and tested in our laboratory. Nowadays, the robustness of the different scoring functions to correctly predict the binding affinity of different ligands versus the corresponding target is very feeble, and this is particularly true in the case of ligand–GPCRs recognition.^{21–24} In this study, we decided to use CoMFA as an “alternative” strategy to quantitatively address the binding properties of our pyrazolotriazolopyrimidine derivatives. In fact, after analyzing docking results, we utilized the superposition of all low energy docked conformations as structural input (supermolecule) for a conventional CoMFA. Both field analysis and quantitative regression model have been used to intrinsically validate the model. As already mentioned above, a remarkable correlation coefficient (cross-validated r^2_{cv}) of 0.840 was obtained. On the basis of our combined approach, we have designed, synthesized, and tested 17 new derivatives. To severely test the quality of our model, we voluntarily designed antagonists with estimated activities from the micromolar to the sub-nanomolar range. Impressively, all predicted K_i values were very close to the experimental values. This is nice evidence that this combined approach is a good integration between a very consolidated target-based approach, such as molecular docking, and a solid quantitative ligand-based methodology such as CoMFA.

Molecular Modeling. 1. Building a Y-Shape Antagonist-Bound Model of Human A₃ Receptor. As already mentioned pyrazolo–triazolo–pyrimidines bearing different substitutions at the N⁵ and N⁸ positions have been described as highly potent and selective human A₃ adenosine receptor antagonists. To perform our *combined* target-based and ligand-based approach, we decided to theoretically depict the putative TM binding motif of pyrazolo–triazolo–pyrimidines on human A₃ receptor. Following our recently reported modeling approaches,^{15,20,25,26} we built an improved model of the human A₃ receptor, using the bovine rhodopsin crystal structure as template,²⁷ which can be considered a further refinement in building the hypothetical binding site of the A₃ receptor antagonists already proposed. Special care had to be given to the second extracellular (E2) loop which in bovine rhodopsin folds back over transmembrane helices limiting the size of the active site.²⁷ As Jacobson and coauthors have already demonstrated, amino acids of this loop could be involved in direct interactions with the ligands.^{28,29} Details of the building model are given in the Experimental Section. As already reported, the recognition of classic A₃ antagonists seems to occur in the upper region of the TM helical bundle. TMs 3, 5, 6, and 7 seem to be crucial for the recognition of both agonists and antagonists. As recently reported by Jacobson and collaborators,³⁰ a number of amino acid residues in the transmembrane domains 3, 5, and the second extracellular loop (EL2) were individually replaced with Ala and other amino acids. These residues are homologous to those that have been predicted in previous molecular modeling studies of adenosine receptor to be involved in the ligand recognition, including His95, Trp243, Ser247, Asn250, and Lys152. To recognize the hypothetical binding motif of this class of human A₃ inhibitors, a molecular docking study has been carried out on all 106 pyrazolotriazolopyrimidine derivatives reported in Table 1. A multidocking protocol implemented by MOE has been utilized in this computational step (see the Experimental Section for details). Unfortunately, but as logically expected, we did not find any robust quantitative correlation between the experimental binding affinity and the theoretical interaction energies based on the scoring function of our docking protocol. However, our goal was to explore if a multidocking protocol could be used to define a target-based pharmacophore model. The first very interesting result obtained from our molecular docking studies is that all pyrazolotriazolopyrimidine derivatives share a common binding motif inside the TM region of human A₃ receptor. Just for simplifying the description of our results, we have selected derivative **5**, as reference ligand. Indeed, the most energetically stable docked conformation is very similar for all the analyzed compounds. As shown in Figure 2, we identified the hypothetical binding site of the pyrazolotriazolopyrimidine moiety surrounded by TMs 3, 5, 6, and 7 with the furan ring and the N⁸-substituents pointing toward the EL2, and the carbamoyl moiety in the 5-position oriented toward the intracellular environment.

Moreover, the furan ring is positioned between TM5 and TM3 whereas the N⁸-substituents are surrounded by TM2 and TM7. We have defined this peculiar and highly conserved binding motif as the Y-shape binding

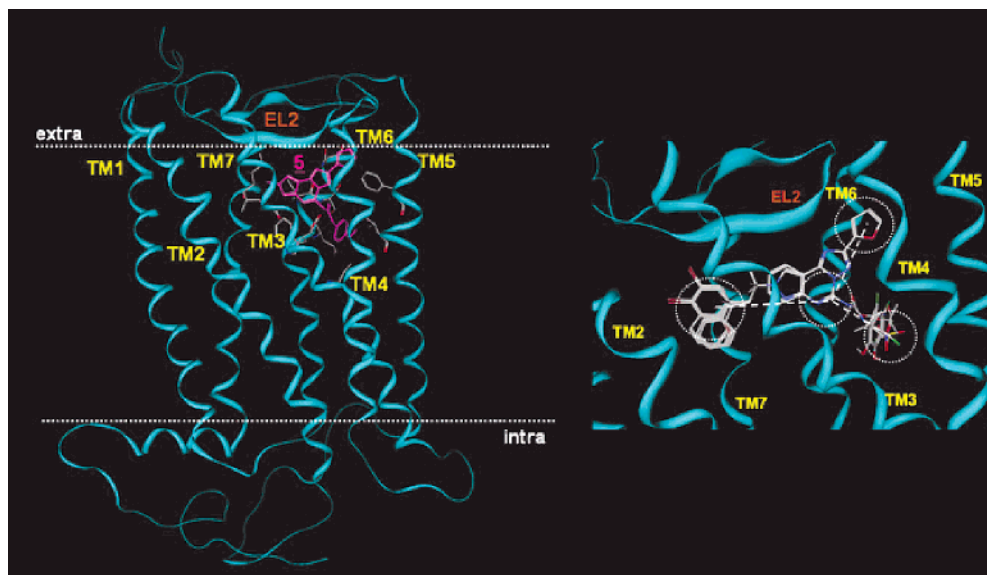


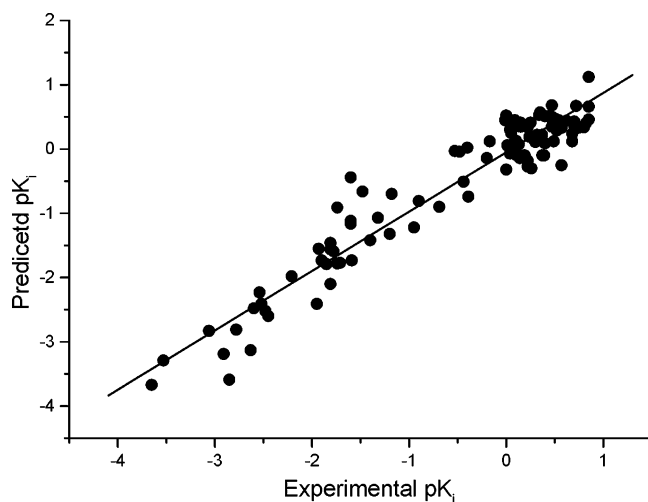
Figure 2. Left: General topology of the human A_3 receptor model. Reference compound **5** (colored in magenta) is docking inside the trans-membrane recognition site (see Experimental Section for details). Side chains of some amino acids important for ligand recognition are highlighted. Right: Side view of the human A_3 receptor TM recognition region. We selected some of our 106 docked antagonists, and we superimposed them to define a new Y-shaped pharmacophore model.

motif. Interestingly, this new target-based pharmacophore model is nicely coherent with all structure–activity relationships already collected on these pyrazolo–triazolo–pyrimidine analogues. Analyzing in detail our model, all pyrazolotriazolopyrimidine derivatives present the carbamoyl moiety in the 5-position surrounded by two polar amino acids: His95 (TM3) and Ser247 (TM6). This region seems to be very critical for the recognition of the antagonist structures. In fact, a major structural difference between the hypothetical binding sites in these receptor subtypes is that the A_3 receptor does not contain the histidine residue in TM6 common to all A_1 (His251 in hA_1) and A_2 (His250 in hA_{2A}) receptors. This histidine has been shown to participate in both agonist and antagonist binding to A_{2A} receptors.³¹ In the A_3 receptor this histidine in TM6 is replaced with a serine residue (Ser247 in hA_3). The stabilizing interactions among the carbamoyl moiety and these polar amino acids orient the carbamoyl phenyl ring in the middle of the TM bundle as clearly shown in Figure 2. In particular, the N–H of His95 (TM3) and the oxygen atom of the carbamoyl group are separated by 2.6 Å and appropriately oriented to form an H-bonding interaction. The side chain of Ser247 (TM6) is within hydrogen-bonding distance of NH of the carbamoyl group at 2.9 Å. According to the recently published mutagenesis results, His95 is crucial for ligand recognition, whereas Ser247 slightly affects the binding of both agonists and antagonists.³⁰ The receptor region around the phenyl ring of the carbamoyl moiety is mostly hydrophobic and characterized by three nonpolar amino acids: Ile98 (TM3), Ile186 (TM5), Leu244 (TM6). This environment could justify why polar substituents at the para position are not very well tolerated, as in the case of sulfonic acid group.¹⁵ Evaluation of the ligand binding pocket of the receptor reveals that very limited empty space is present between TM5 and TM6 and, consequently, a steric control seems to take place around the para position of the phenyl ring. As already demonstrated, substituents at the para position of the N^5 -

phenyl ring induce a decrease of affinity at the human A_3 adenosine receptors of about 2–5-fold with respect to the unsubstituted derivatives.^{15,26} The same steric control takes place when substituents larger than hydrogen are present at the meta position of the phenyl ring. In this case a strong steric repulsion among substituents, at the meta position, and amino acid side chains of TM6 and TM7 could significantly reduce the affinity at the hA_3 receptor. On the contrary, substituents at the ortho position seem to occupy an empty region of the binding cavity. As previously described, in the chloro substituted series the change of the position (2- or 4-substitution) seems not to influence affinity at the hA_1 , hA_{2A} , and hA_{2B} receptors compared to the 3-chloro substituted compounds, maintaining it in the high nanomolar range (100–500 nM), while significant differences appeared in binding affinity to the hA_3 adenosine receptors (see Table 1).¹⁵

Another important and highly conserved interaction, probably a π – π interaction, is predicted among the furan ring of the pyrazolotriazolopyrimidine analogues and the two phenylalanine residues, Phe168 (EL2) and Phe182 (TM5), respectively. This interaction seems to be another important pharmacophore feature of our binding motif. Interestingly, the amino acids corresponding to Leu90 and Phe182 in the human A_{2A} receptor were found to be essential for the binding of both agonists and antagonists.^{31,32}

Moreover, another important and peculiar hydrophobic pocket delimited by nonpolar amino acids, Leu90 (TM3), Leu246 (TM6), and Ile268 (TM7), is also addressable in our binding site model. According to our docking studies, all the substituents at the N^8 position are located within this region of the receptor according to our binding hypothesis. However, two hydrophilic amino acids, such as Ser175 (EL2) and His272 (TM7), are present on the border of this hydrophobic pocket, and they can interact through hydrogen bonding in the presence of appropriate substituents. We have already

Table 2. Statistics of the Calibration Human A₃ CoMFA Model

no. of compounds	106
principal components ^a	6
r^2_{cv} ^b	0.840
r^2	0.922
F -test ^c	141.67
p	<0.001
r^2_{bs} ^d	0.802
steric contribution	0.571
electrostatic contribution	0.429
SEP ^e	0.185
std dev ^f	0.022

^a Minimum $s = 2.0$. ^b Standard error of prediction (cross-validated) = $(PRESS/(n - c - l))^{1/2}$, n = number of rows, c = number of components. ^c Ratio of r^2 explained to unexplained = $r^2/(l - r^2)$. ^d $r^2_{bs} = r^2$ after bootstrapping. ^e Cross-validated r^2 after leave-one-out procedure: $r^2_{cv} = (SD - PRESS)/SD$, $SD = (Y_{actual} - Y_{mean})^2$ and $PRESS = \sum(Y_{predicted} - Y_{actual})$. For further explanation of these mathematical formulas, see ref 40. ^f The std dev row belongs with the bootstrapping r^2 .

published and rationalized that hydrophobic substituents are very well tolerated at the N⁸ position.¹⁸

Finally, a strong hydrogen bonding interaction is possible between Asn250 (TM6) and the triazolo ring of the pyrazolotriazolopyrimidine moiety. In particular, the N–H of Asp250 and the N⁴ of the triazolo ring group are separated by 2.5 Å and appropriately oriented to form an H-bonding interaction. Also this asparagine residue, conserved among all adenosine receptor subtypes, was found to be important for ligand binding.^{31,32}

No direct interactions are predicted between the antagonist structure and the two polar amino acids Thr94 (TM3) and Ser97 (TM3). As previously reported, the corresponding two amino acids in the A₁ and A_{2A} receptors, respectively, are important for the coordination of agonists, but not for antagonists.^{31,32}

Molecular Modeling. 2. CoMFA as “Alternative” Scoring Function. In tandem with our molecular docking studies, a CoMFA methodology was applied to the data from the A₃ binding assay as a means of identifying the structural features of pyrazolotriazolopyrimidine derivatives responsible for affinity. Our approach consists of utilizing CoMFA as a quantitative tool to predict the receptor binding affinity using the pharmacophore model based on the multidocking approach described above. PLS was used in conjunction with cross-validation to obtain the optimal number of components to be used in the subsequent analyses. PLS

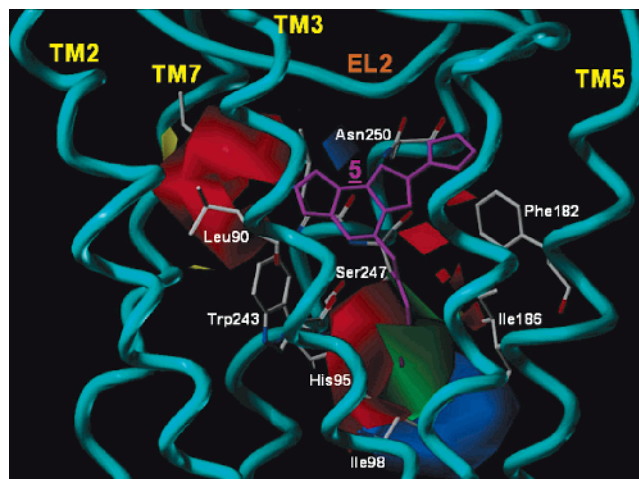
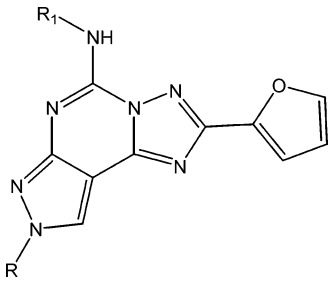


Figure 3. Side view of the 5–A₃ complex model. The side chains of some crucial important residues in proximity (≤ 5 Å) to the docked pyrazolo–triazolo–pyrimidine molecule are highlighted and labeled: Leu90 (TM3), His 95 (TM3); Phe182 (TM5), Ile186 (TM5); Trp243 (TM6); Ser247 (TM6), Asn250 (TM6), Ser271 (TM7), His272 (TM7), Ser275 (TM7). The steric and the electrostatic contour plots, obtained from the CoMFA analysis, are included into ligand binding cavity. The yellow and the blue polyhedra correspond to regions of the field that are predicted to decrease the A₃ receptor affinity, while the green and the red regions are predicted to increase binding affinity.

analysis based on a least-squares fit gave a correlation with a cross-validated r^2_{cv} of 0.840, with the maximum number of components set equal to 6 (maximum number of components set equal to 4, 5, or 7 gave lower cross-validated r^2_{cv}) and the cross-validation groups set equal to the number of observations. The non-cross-validated PLS analysis was repeated with the optimum number of components, as determined by the cross-validated analysis, to give an r^2 of 0.922. To obtain statistical confidence limits, the non-cross-validated analysis was repeated with 10 bootstrap groups, which yielded an r^2 of 0.802 (optimum number of components was 6), SEP = 0.185, standard deviation = 0.022, steric contribution = 0.571, and electrostatic contributions = 0.429. The CoMFA-derived QSAR of pyrazolotriazolopyrimidine derivatives exhibited a good cross-validated correlation, indicating that it was highly predictive. Cross-validation provides information concerning the predictive ability of the QSAR data set by minimizing the occurrence of chance correlations in the QSAR model. The high bootstrapped r^2 value and a small standard deviation suggest a high degree of confidence in the analysis. Fitted vs measured pK_i values for the CoMFA analysis of the human A₃ training set are shown in Table 2.

The coefficients corresponding to each sampled field point in the resulting correlation equation were graphically contoured. Contours corresponding to the steric (green and yellow) and electrostatic (blue and red) fields are plotted together with compound 5 docked inside the human A₃ binding cavity as shown in Figure 3.

The polyhedra describe the regions of space where the steric and the electrostatic fields are predicted by the CoMFA model to have the greatest effect on binding affinity. The yellow and the blue polyhedra correspond to regions of the field that are predicted to decrease the A₃ receptor affinity, while the green and the red regions are predicted to increase binding affinity. As shown in

Table 3. Structures, Physicochemical Parameters, and Human A₃ (Predicted and Calculated) Binding Affinities of New Synthesized Compounds (**107–123**)


no.	R	R ¹	mp (°C)	MW	hA ₃ K _i (nM)	
					obsd	calcd
107	<i>n</i> -C ₈ H ₁₇	H	135	353.20	2050 (1570–2680)	3288
108	CH ₂ - <i>c</i> -C ₆ H ₁₁	H	195	337.17	1720 (1320–2240)	1380
109	CH ₃	CONH- <i>c</i> -C ₆ H ₁₁	208–210	380.17	1.01 (0.89–1.16)	0.93
110	CH ₃	CONH- <i>n</i> -C ₅ H ₁₁	185–188	368.17	1.95 (1.39–2.72)	0.33
111	CH ₃	CONH-Ph-4-CH ₂ CO ₂ Et	222–224	461.17	0.82 (0.59–1.15)	0.45
112	CH ₂ CH ₂ CH(CH ₃) ₂	CONH- <i>c</i> -C ₆ H ₁₁	165	436.23	20.53 (17.65–28.76)	20.70
113	CH ₂ CH ₂ CH(CH ₃) ₂	CONH- <i>n</i> -C ₅ H ₁₁	178–180	424.23	8.09 (7.46–8.78)	7.39
114	CH ₂ CH ₂ CH(CH ₃) ₂	CONH-Ph-4-CH ₂ CO ₂ Et	163	516.22	11.89 (8.72–16.20)	9.95
115	CH ₂ CH ₂ CH(CH ₃) ₂	CONH-Ph-4-CH ₃	223–228	440.20	7.41 (5.56–9.86)	7.28
116	<i>n</i> -C ₈ H ₁₇	CONH- <i>c</i> -C ₆ H ₁₁	123–125	478.28	16.29 (13.74–19.30)	17.06
117	<i>n</i> -C ₈ H ₁₇	CONH- <i>n</i> -C ₅ H ₁₁	125	466.28	7.83 (4.89–12.53)	6.10
118	<i>n</i> -C ₈ H ₁₇	CONH-Ph-4-CH ₂ CO ₂ Et	150–154	558.27	9.97 (8.29–11.98)	8.20
119	<i>n</i> -C ₈ H ₁₇	CONH-Ph-4-CH ₃	226–228	486.25	4.48 (3.65–5.50)	3.09
120	CH ₂ - <i>c</i> -C ₆ H ₁₁	CONH- <i>c</i> -C ₆ H ₁₁	130	462.25	6.70 (5.30–8.46)	7.21
121	CH ₂ - <i>c</i> -C ₆ H ₁₁	CONH- <i>n</i> -C ₅ H ₁₁	170	450.25	3.98 (3.16–5.01)	2.58
122	CH ₂ - <i>c</i> -C ₆ H ₁₁	CONH-Ph-4-CH ₂ CO ₂ Et	185	542.24	6.95 (5.34–9.06)	3.48
123	CH ₂ - <i>c</i> -C ₆ H ₁₁	CONH-Ph-4-CH ₃	206–210	470.22	5.94 (4.36–8.10)	2.54

Figure 3, the proposed pharmacophore model fits very nicely within the transmembrane binding cleft. All steric and electrostatic features are coherent with the structure–activity relationship already described during the molecular docking analysis above. In particular, a green polyhedron, with a mean steric bulk favorable region, is found near the N⁵-carbamoyl moiety. As already described, this green polyhedron nicely fits with the receptor region around the phenyl ring of the carbamoyl moiety and characterized by three nonpolar amino acids: Ile98 (TM3), Ile186 (TM5), Leu244 (TM6). Moreover, from an electrostatic point of view the two red polyhedra around to N⁸-substituents and to the N⁵-carbamoyl moiety are complementary respectively to Ser175 (EL2), His95 (TM3), Ser247 (TM6), and His272 (TM7). On the other hand, the blue polyhedron close to the N⁵-phenyl ring is surrounded by four nonpolar amino acids [Ile98 (TM3), Ile186 (TM5), Phe239 (TM6), and Leu244 (TM6)] and the most important electrostatic interactions are mediated by the corresponding CO–NH peptide bonds.

Molecular Modeling. 3. Validation Set. On the basis of both the target-based pharmacophore model and the CoMFA model as alternative scoring function, we have designed, synthesized, and tested 17 (**107–123**) new derivatives with a different spectrum of affinity at the human A₃ receptor. Compounds **107–123** (test set, shown in Table 2) were used to evaluate the predictive power of this CoMFA model. As in the calibration step, a good predictive ability with an $r^2_{\text{pred}} = 0.873$ for the compounds in the test set was obtained. Table 3 shows that the affinities of all the examined compounds were predicted within 0.25 log unit across a range of 2.00 log units. Impressively, the predicted K_i values were very close to the experimental values. In particu-

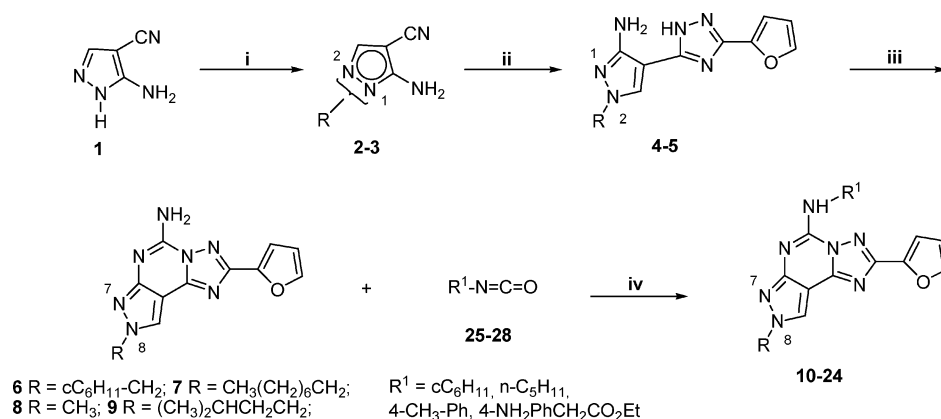
lar, derivative **111** (4-[3-(2-furan-2-yl-8-methyl-8H-pyrazolo[4,3-*e*][1,2,4]triazolo[1,5-*c*]pyrimidin-5-yl)ureido]-phenylacetic acid ethyl ester) is active in a sub-nanomolar range (0.82 nM) as correctly predicted by our regression model. Again, this is clear evidence that this combined approach is a nice integration between a very consolidated target-based approach, such as molecular docking, and a solid quantitative ligand-based methodology such as CoMFA.

Synthesis of the Validation Set. Compounds **107–123** were prepared following the general synthetic strategy summarized in Scheme 1. Compounds **107–123** were synthesized according to a well-known procedure for the synthesis of the pyrazolo[4,3-*e*]-1,2,4-triazolo[1,5-*c*]pyrimidines, previously reported.^{14–18}

Alkylation of 5-amino-4-cyanopyrazole **124** with the appropriate alkyl halide in dry dimethylformamide led to an approximately 1:4 mixture of the N¹ and N² regioisomers (**125**, **126**) as an inseparable mixture, used for the following steps without any further purification.

Pyrazoles (**125** and **126**) were reacted with 2-furoic acid hydrazide in diphenyl ether at 260 °C to yield the aminotriazoles **127** and **128**, which were in turn converted into the 5-amino-8-(substituted)-2-(2-furyl)-pyrazolo[4,3-*e*]-1,2,4-triazolo[1,5-*c*]pyrimidine derivatives by reaction with cyanamide in the presence of *p*-toluenesulfonic acid. After separation of N⁷ (minor product) and N⁸ (major product) regioisomers by flash chromatography, the dried compounds **107** and **108** were obtained in good overall yield. Final compounds **109–123** were obtained by reaction of amino compounds **5**, **20**, **107**, and **108**, with the appropriate isocyanate (**129–132**) in dioxane at reflux.

Final Remarks. Fundamental understanding of the molecular details of ligand/GPCR interactions remains

Scheme 1^a

^a Reagents: (i) NaH, DMF, RX; (ii) 2-furoic hydrazide, Ph₂O, 260 °C; (iii) NH₂CN, 1-methyl-2-pyrrolidone, pTsOH, 140 °C, then flash chromatography; (iv) dioxane reflux, 18 h. For compounds **8** and **9** see ref 18.

very rudimentary. How agonist binding transforms a resting GPCR into its active form and the microscopic basis of binding site blockade by an antagonist are generally still unclear. We decided to utilize in *tandem* structure-based and ligand-based drug design strategies to improve our knowledge about the human A₃ receptor–antagonist recognition process. In particular, using this combined strategy we have identified common subtle structural features of pyrazolo–triazolo–pyrimidines which lead to enhanced potency or selectivity at A₃ receptors. To specifically address the hypothetical binding motif of pyrazolotriazolopyrimidine derivatives we have used a multiple docking strategy to identify a novel target-based pharmacophore model. Superimposition of all low energy docked conformations has been used to characterize the more conserved chemical features crucial to the recognition process (target-based pharmacophore) and their fit in the putative binding site of the receptor. On the basis of the proposed pharmacophore map, we can state that the receptor binding properties of different A₃ antagonist derivatives are due to recognition at a common region inside the receptor binding site and, consequently, a common electrostatic potential profile. Due to the poor predictivity of the current scoring functions, we have decided to use CoMFA as an alternative tool to quantitatively predict the ligand–receptor binding affinity. Consistently with this new combined pharmacophore hypothesis, we have designed, synthesized, and tested 17 new pyrazolotriazolopyrimidine derivatives with a different spectrum of affinity at the human A₃ receptor. As already underlined, the predicted pK_i values were very close to the experimental values.

In conclusion, using our combined approach pyrazolo–triazolo–pyrimidine derivatives have served as structural scaffolds for enhancement of selectivity at human A₃ receptors and as important modeling probes for the study of the human A₃ receptor binding site. Moreover, we are deeply analyzing whether or not structurally unrelated antagonists would fit into the novel defined pharmacophore model.

Experimental Section

Computational Methodologies. All molecular modeling studies were carried out on a 6 CPU (PIV 2.0–3.0 GHz) Linux cluster running under openMosix architecture.³³

Homology modeling, energy calculation, and docking studies have been done using Molecular Operating Environment (MOE, version 2003.03) suite.³⁴

CoMFA is a three-dimensional QSAR method that operates on a set of ligands that have been superimposed to reflect their anticipated common receptor binding orientation. CoMFA models describe the extent to which the change in magnitude of the electrostatic and steric fields as a function of compound, sampled as a function of spatial position around the compound set, accounts for the variance in measured biological activity. CoMFA studies were performed on a Silicon Graphics Power Indigo2 R8000 workstation running SYBYL 6.5.³⁵ Quantum calculations used throughout this study were performed using MOPAC (version 7.0).³⁶

Homology Model of the Resting State of Human A₃ Receptor. On the basis of the assumption that GPCRs share similar TM boundaries and overall topology,³⁷ a homology model of the human A₃ receptor was constructed. First, the amino acid sequences of TM helices of the resting state A₃ receptor were aligned with those of bovine rhodopsin, guided by the highly conserved amino acid residues, including the DRY motif (D3.49, R3.50, and Y3.51) and three Pro residues (P4.60, P6.50, and P7.50) in the TM segments of GPCRs. The same boundaries were applied for the TM helices of the A₃ receptor as were identified from the X-ray crystal structure for the corresponding sequences of bovine rhodopsin,²⁷ the C_α coordinates which were used to construct the seven TM helices for the human A₃ receptor. The loop domains of the human A₃ receptor were constructed by the loop search method implemented in MOE. In particular, loops are modeled first, in random order. For each loop, a contact energy function analyzes the list of candidates collected in the segment searching stage, taking into account all atoms already modeled and any atom specified by the user as belonging to the model environment. These energies are then used to make a Boltzmann-weighted choice from the candidates, the coordinates of which are then copied to the model. Any missing side chain atoms are modeled using the same procedure. Side chains belonging to residues whose backbone coordinates were copied from a template are modeled first, followed by side chains of modeled loops. Outgaps and their side chains are modeled last. Special caution had to be given to the second extracellular (E2) loop, which has been described in bovine rhodopsin to fold back over transmembrane helices,²⁷ and, therefore, it limits the size of the active site. Hence, amino acids of this loop could be involved in direct interactions with the ligands. The presence of a disulfide bridge between cysteines in TM3 and E2 might be the driving force to this peculiar fold of the E2 loop. Since this covalent link is conserved in all receptors modeled in the current study, the E2 loop was modeled using a rhodopsin-like constrained geometry around the E2–TM3 disulfide bridge. After the heavy atoms were modeled, all hydrogen atoms were added, and the protein coordinates were then

minimized with MOE using the AMBER94 force field.³⁸ The minimizations were carried out by 1000 steps of steepest descent followed by conjugate gradient minimization until the rms gradient of the potential energy was less than 0.1 kcal mol⁻¹ Å⁻¹.

Molecular Docking (Multidocking) of the Human A₃ Receptor Antagonists. All 106 antagonist structures were docked into the hypothetical TM binding site by using the MULTIDOCK docking program, which is part of the MOE suite. Conformational samplings were conducted within a user-specified 3D docking box, using the Tabu Search protocol³⁹ and MMFF94 force field.⁴⁰ MOE-Dock performs a user-specified number of independent docking runs (20 in our specific case) and wrote the resulting conformations and their energies in a molecular database file. The resulting docked complexes were subjected to MMFF94 energy minimization until the rms of the conjugate gradient was <0.1 kcal mol⁻¹ Å⁻¹. Charges for the ligands were imported directly from the MMFF94 force field.

The interaction energy values were calculated as follows: $\Delta E_{\text{binding}} = E_{\text{complex}} - (E_{\text{ligand}} + E_{\text{receptor}})$. These energies are not rigorous thermodynamic quantities, but can only be used to compare the relative stabilities of the complexes. Therefore, these interaction energy values cannot be used to calculate binding affinities since changes in entropy and solvation effects are not taken into account.

CoMFA: Data Sets and Binding Studies. A total of 106 pyrazolo-triazolo-pyrimidine derivatives were included in the training set used to generate the CoMFA model for human A₃ receptors (see Table 1).

The synthesis of all pyrazolo-triazolo-pyrimidine derivatives was reported in detail previously.^{15–20} Binding of [³H]MRE3008-F20 to CHO cells transfected with the human recombinant A₃ adenosine receptors was performed according to Varani et al.⁴¹ Competition experiments were carried out in duplicate in a final volume of 250 μL in test tubes containing 1 nM [³H] MRE3008-F20, 50 mM Tris HCl buffer, 10 mM MgCl₂, pH 7.4, 100 μL of diluted membranes (50 μg protein/assay), and at least 6–8 different concentrations of examined ligands. Incubation time was 120 min at 4 °C, according to the results of previous time-course experiments.⁴¹ Nonspecific binding was defined as binding in the presence of 1 μM MRE3008-F20 and was about 25% of total binding. Bound and free radioactivity were separated by filtering the assay mixture through Whatman GF/B glass-fiber filters using a Micro-Mate 196 cell harvester (Packard Instrument Company). The filter bound radioactivity was counted on Top Count (efficiency 57%) with Micro-Scint 20. The protein concentration was determined according to the Bio-Rad method with bovine albumin as reference standard.⁴²

CoMFA: Molecular Superposition. The pyrazolo-triazolo-pyrimidine moiety is believed to be a determinant key for binding interactions of described derivatives. The energetically more stable docking conformation has been used for all compounds, as input for the CoMFA field calculations.

CoMFA: Field Calculations and Regression Techniques. The electrostatic and steric fields were sampled along a three-dimensional lattice encompassing all molecules in each receptor data set. The lattice consisted of 720 sample points based on a 2.0 Å lattice spacing with boundaries extending 4.0 Å beyond the largest structure in all directions. Lattice spacings of 0.75 and 1.5 Å were also used without improvements of the CoMFA results. The lattice points within the union volume of the superimposed structures were dropped. The probe used to calculate the CoMFA fields consisted of an sp³ carbon atom with a +1 charge and a van der Waals radius of 1.52 Å. The steric and electrostatic fields were calculated separately for each molecule using respectively a Lennard-Jones 6–12 potential and a Coulombic potential with a 1/*r* distance-dependent dielectric. The steric and electrostatic energies were truncated at 30 kcal/mol. The field values corresponding to the 720 sample points for each molecule, together with binding affinity data, were stored in a SYBYL Molecular Spreadsheet to facilitate statistical analysis.

Partial least squared (PLS) regression analysis⁴³ was performed on the human A₃ antagonist dataset using a subset of CoMFA field sample points falling with a standard deviation ≤1.0 kcal/mol. The steric and the electrostatic fields were scaled to equalize their weighting in the CoMFA models (SYBYL command “scaling CoMFA_std”). PLS was performed using cross-validation to evaluate the predictive ability of the CoMFA models.⁴⁴ The optimal number of latent variables came from the cross-validation equation having the lowest standard error, and a significance level ≥99.5% was estimated using the stepwise *F*-test. Bootstrap analysis of the dataset was used to evaluate the statistical confidence limits of the results.⁴⁴ A σ value of 2.0 was adopted for both the cross-validated and non-cross-validated analysis. σ values of 1.0 or 0.5 did not significantly change the calculated *r*².

Initial PLS analyses were performed in conjunction with the cross-validation option (leave-one-out method) to obtain the optimal number of components to be used in the subsequent analyses of the dataset. The PLS analysis was repeated with the number of cross-validation groups set to zero. The optimal number of components was designated as that which yielded the highest cross-validated *r*² values in the non-cross-validated (conventional) analyses. The final PLS analysis with 10 bootstrap groups and the optimal number of components was performed on the complete dataset.

The corresponding calibration equation (resulting from the simultaneous contribution of all the observations) was derived after the optimal dimensionality of each receptor model was established, by PLS analysis and cross-validation. The calibration equation with latent variables was then converted to the original parametric space represented by probe–ligand interaction energies. A 3D-QSAR whose coefficients were associated with statistically significant lattice locations was therefore derived. CoMFA coefficient contour maps were generated by interpolation of the pairwise products between the 3D-QSAR coefficients and the standard deviations of the associated energy variables.

CoMFA: Test Sets. The test sets consisted of 17 new synthesized molecules for the considered training set **107–123** (Table 2). These structures were chosen to maximize a uniform sampling of biological activity. All predicted activities for the test set molecules were calculated using the optimized CoMFA model. The results of the non-cross-validated calibration model on the test sets are summarized in Table 2.

CoMFA: “Predictive” *r*² Values. The “predictive” *r*²_{pred} was based only on molecules not included in the training set and is defined as explained by Marshall and co-workers.⁴⁵

Chemistry. General. Reactions were routinely monitored by thin-layer chromatography (TLC) on silica gel (precoated F₂₅₄ Merck plates) and products visualized with iodine or potassium permanganate solution. Infrared spectra (IR) were measured on a Jasco FT-IR 200 spectrophotometer. ¹H NMR were determined in CDCl₃ or DMSO-*d*₆ solutions with a Varian Gemini 200 spectrometer, peaks positions are given in parts per million (δ) downfield from tetramethylsilane as internal standard, and *J* values are given in hertz. Light petroleum ether refers to the fractions boiling at 40–60 °C. Melting points were determined on a Buchi-Tottoli instrument and are uncorrected. Chromatographies were performed using Merck 60–200 mesh silica gel. All products reported showed IR and ¹H NMR spectra in agreement with the assigned structures. Organic solutions were dried over anhydrous magnesium sulfate. Elemental analyses were performed by the micro-analytical laboratory of Dipartimento di Chimica, University of Trieste, and were within ±0.4% of the theoretical values for C, H, and N.

General Procedures for the Preparation of 8-(Ar)alkyl-2-(2-furyl)pyrazolo[4,3-*e*]1,2,4-triazolo[1,5-*c*]pyrimidine (107, 108). A solution of **124** (10 mmol) in 40 mL of DMF cooled to 0 °C was treated with NaH (60% in oil, 12 mmol) in several portions over 10 min. After 45 min, the appropriate alkyl halide (12 mmol) was added and the reaction mixture was allowed to warm to 25 °C and stirred for 3–5 h (TLC:EtOAc 1:1). The reaction was quenched by addition of H₂O (80 mL),

and the aqueous layer was extracted with EtOAc (5 × 25 mL). The organic layers were recombined, dried (Na₂SO₄), filtered, and concentrated at reduced pressure, to afford the alkylated pyrazole (**125**, **126**) as an inseparable mixture of N¹ and N² isomers (ratio approximately 1:4). This mixture of N¹- and N²-substituted-4-cyano-5-amino pyrazoles (**125**, **126**) was then dissolved in diphenyl ether (50 mL), and 2-furoic acid hydrazide (13 mmol) was added. The mixture was heated at 260 °C using a Dean–Stark trap for the azeotropic elimination of water produced in the reaction. After 2.5 h, the mixture was poured onto hexane (300 mL) and cooled. The precipitate of crude pyrazole–triazole derivatives (**127**, **128**) was filtered off and utilized for the next step without further purifications. The crude residue was dissolved in *N*-methylpyrrolidone (40 mL), cyanamide (60 mmol) and *p*-toluenesulfonic acid (15 mmol) were added, and the mixture was heated at 160 °C for 4 h. Cyanamide (60 mmol) was added again, and the solution was heated overnight. Then the solution was diluted with EtOAc (80 mL) and the precipitate (excess of cyanamide) was filtered off; the filtrate was concentrated under reduced pressure and washed with water (3 × 30 mL). The organic layer was dried (Na₂SO₄) and evaporated under vacuum. The residue was purified by flash chromatography (EtOAc/light petroleum 3:7) for obtaining the major product (N⁸ alkylated) (**107**, **108**), which was obtained in a good overall yield.

5-Amino-8-*n*-octyl-2-(2-furyl)-pyrazolo[4,3-*e*]1,2,4-triazolo[1,5-*c*]pyrimidine (107). Yield: 45%; pale brown solid. IR (KBr): 3430–2950, 1680, 1655, 1620, 1550, 1450 cm⁻¹. ¹H NMR (DMSO-*d*₆) δ: 0.78 (t, 2H, *J* = 7); 1.01–1.25 (m, 10H); 1.62–1.99 (m, 2H); 4.22 (t, 2H, *J* = 7); 6.67 (dd, 1H, *J* = 2, *J* = 4); 7.14 (d, 1H, *J* = 4); 7.57 (bs, 2H); 7.88 (d, 1H, *J* = 2); 8.58 (s, 1H). Anal. (C₁₈H₂₃N₇O) C, H, N.

5-Amino-8-cyclohexylmethyl-2-(2-furyl)pyrazolo[4,3-*e*]1,2,4-triazolo[1,5-*c*]pyrimidine (108). Yield: 38%; pale brown solid. IR (KBr): 3445–2960, 1675, 1650, 1615, 1555, 1450 cm⁻¹. ¹H NMR (DMSO-*d*₆) δ: 0.89–1.08 (m, 4H); 1.43–1.49 (m, 4H); 1.71–1.89 (m, 1H); 4.08 (d, 2H, *J* = 6); 6.68 (dd, 1H, *J* = 2, *J* = 4); 7.14 (d, 1H, *J* = 4); 7.58 (bs, 2H); 7.89 (d, 1H, *J* = 2); 8.54 (s, 1H). Anal. (C₁₇H₁₉N₇O) C, H, N.

General Procedure for the Preparation of 5-[[Substituted]amino]carbonylamino-8-alkyl-2-(2-furyl)pyrazolo[4,3-*e*]1,2,4-triazolo[1,5-*c*]pyrimidine (109–123). Amino compound (**5**, **20**, **107**, **108**) (10 mmol) was dissolved in freshly distilled dioxane (15 mL), and the appropriate isocyanate (**129–132**) (13 mmol) was added. The mixture was refluxed under argon for 18 h. Then the solvent was removed under reduced pressure, and the residue was purified by flash chromatography (EtOAc–light petroleum 7:3) to afford the desired compounds **109–123**.

5-[[Cyclohexyl]amino]carbonylamino-8-methyl-2-(2-furyl)pyrazolo[4,3-*e*]1,2,4-triazolo[1,5-*c*]pyrimidine (109). Yield: 90%; white solid. IR (KBr): 3245–2950, 1675, 1615, 1600, 1520 cm⁻¹. ¹H NMR (CDCl₃) δ: 1.01–1.95 (m, 10H); 3.26–3.29 (m, 1H); 4.06 (s, 3H); 6.68 (dd, 1H, *J* = 2, *J* = 4); 7.25 (d, 1H, *J* = 4); 7.94 (d, 1H, *J* = 2); 8.72 (s, 1H); 8.73 (bs, 1H); 9.01 (bs, 1H). Anal. (C₁₈H₂₀N₈O₂) C, H, N.

5-[[*n*-Pentyl]amino]carbonylamino-8-methyl-2-(2-furyl) pyrazolo[4,3-*e*]1,2,4-triazolo[1,5-*c*]pyrimidine (110). Yield: 82%; white solid. IR (KBr): 3240–2970, 1670, 1620, 1600, 1510 cm⁻¹. ¹H NMR (CDCl₃) δ: 0.88 (t, 3H, *J* = 7); 1.10–1.51 (m, 6H); 3.26–3.29 (m, 1H); 4.09 (s, 3H); 6.72 (dd, 1H, *J* = 2, *J* = 4); 7.26 (d, 1H, *J* = 4); 7.96 (d, 1H, *J* = 2); 8.72 (s, 1H); 8.73 (bs, 1H); 8.98 (bs, 1H). Anal. (C₁₇H₂₀N₈O₂) C, H, N.

4-[3-(2-Furan-2-yl-8-methyl-8*H*-pyrazolo[4,3-*e*]1,2,4-triazolo[1,5-*c*]pyrimidin-5-yl)ureido]phenylacetic Acid Ethyl Ester (111). Yield: 82%; pale gray solid. IR (KBr): 3250–2960, 1725, 1675, 1615, 1600, 1510 cm⁻¹. ¹H NMR (CDCl₃) δ: 1.23 (t, 3H, *J* = 7); 3.62 (s, 2H); 4.16 (q, 2H, *J* = 7); 6.72 (dd, 1H, *J* = 2, *J* = 4); 7.17 (d, 2H, *J* = 9); 7.26 (d, 1H, *J* = 4); 7.71 (d, 2H, *J* = 7); 7.76 (d, 1H, *J* = 2); 8.15 (s, 1H); 8.56 (bs, 1H); 11.13 (bs, 1H). Anal. (C₂₂H₂₁N₈O₄) C, H, N.

5-[[Cyclohexyl]amino]carbonylamino-8-isopentyl-2-(2-furyl)pyrazolo[4,3-*e*]1,2,4-triazolo[1,5-*c*]pyrimidine (112).

Yield: 87%; white solid. IR (KBr): 3250–2970, 1673, 1610, 1600, 1515 cm⁻¹. ¹H NMR (CDCl₃) δ: 0.88 (d, 6H, *J* = 6); 1.15–1.99 (m, 13H); 3.61–3.63 (m, 1H); 4.21 (t, 2H, *J* = 7); 6.65 (dd, 1H, *J* = 2, *J* = 4); 7.23 (d, 1H, *J* = 4); 7.97 (d, 1H, *J* = 2); 8.64 (bs, 1H); 8.81 (s, 1H); 9.00 (bs, 1H). Anal. (C₂₂H₂₈N₈O₂) C, H, N.

5-[[*n*-Pentyl]amino]carbonylamino-8-isopentyl-2-(2-furyl)pyrazolo[4,3-*e*]1,2,4-triazolo[1,5-*c*]pyrimidine (113). Yield: 87%; white solid. IR (KBr): 3245–2955, 1675, 1625, 1600, 1510 cm⁻¹. ¹H NMR (CDCl₃) δ: 0.79–0.99 (m, 9H); 1.11–1.59 (m, 11H); 1.64–1.81 (m, 2H); 4.35 (t, 2H, *J* = 7); 6.68 (dd, 1H, *J* = 2, *J* = 4); 7.25 (d, 1H, *J* = 4); 7.94 (d, 1H, *J* = 2); 8.63 (bs, 1H); 8.81 (s, 1H); 9.02 (bs, 1H). Anal. (C₂₁H₂₈N₈O₂) C, H, N.

4-[3-(2-Furan-2-yl-8-isopentyl-8*H*-pyrazolo[4,3-*e*]1,2,4-triazolo[1,5-*c*]pyrimidin-5-yl)ureido]phenylacetic Acid Ethyl Ester (114). Yield: 68%; pale brown solid. IR (KBr): 3230–2950, 1723, 1670, 1625, 1600, 1500 cm⁻¹. ¹H NMR (CDCl₃) δ: 0.96 (d, 6H, *J* = 6); 1.23 (t, 3H, *J* = 7); 1.25–1.28 (m, 1H); 3.59 (s, 1H); 4.19 (t, 2H, *J* = 7); 4.39 (q, 2H, *J* = 7); 6.61 (dd, 1H, *J* = 2, *J* = 4); 7.17 (d, 2H, *J* = 9); 7.30 (d, 1H, *J* = 4); 7.61 (d, 2H, *J* = 7); 7.65 (d, 1H, *J* = 2); 8.21 (s, 1H); 8.57 (bs, 1H); 11.12 (bs, 1H). Anal. (C₂₆H₂₈N₈O₄) C, H, N.

5-[[4-Tolyl]amino]carbonylamino-8-isopentyl-2-(2-furyl)pyrazolo[4,3-*e*]1,2,4-triazolo[1,5-*c*]pyrimidine (115). Yield: 81%; pale yellow solid. IR (KBr): 3235–2945, 1672, 1620, 1600, 1505 cm⁻¹. ¹H NMR (CDCl₃) δ: 0.96 (d, 6H, *J* = 6); 1.16–1.22 (m, 1H); 1.89–1.92 (m, 2H); 2.32 (s, 3H); 4.39 (t, 2H, *J* = 7); 6.59 (dd, 1H, *J* = 2, *J* = 4); 7.14 (d, 2H, *J* = 9); 7.25 (d, 1H, *J* = 4); 7.54 (d, 2H, *J* = 9); 7.64 (d, 1H, *J* = 2); 8.21 (s, 1H); 8.56 (bs, 1H); 11.01 (bs, 1H). Anal. (C₂₃H₂₄N₈O₂) C, H, N.

5-[[Cyclohexyl]amino]carbonylamino-8-*n*-octyl-2-(2-furyl)pyrazolo[4,3-*e*]1,2,4-triazolo[1,5-*c*]pyrimidine (116). Yield: 80%; white solid. IR (KBr): 3235–2945, 1665, 1615, 1560 cm⁻¹. ¹H NMR (CDCl₃) δ: 0.80 (t, 3H, *J* = 7); 1.01–2.00 (m, 22H); 3.59–3.62 (m, 1H); 4.32 (t, 2H, *J* = 7); 6.72 (dd, 1H, *J* = 2, *J* = 4); 7.25 (d, 1H, *J* = 4); 7.95 (d, 1H, *J* = 2); 8.68 (bs, 1H); 8.78 (s, 1H); 8.99 (bs, 1H). Anal. (C₂₅H₃₄N₈O₂) C, H, N.

5-[[*n*-Pentyl]amino]carbonylamino-8-*n*-octyl-2-(2-furyl)pyrazolo[4,3-*e*]1,2,4-triazolo[1,5-*c*]pyrimidine (117). Yield: 78%; white solid. IR (KBr): 3250–2970, 1663, 1610, 1545 cm⁻¹. ¹H NMR (CDCl₃) δ: 0.78–0.84 (m, 6H); 1.04–1.32 (m, 16H); 1.42–1.50 (m, 2H); 1.79–1.98 (m, 2H); 4.38 (t, 2H, *J* = 7); 6.69 (dd, 1H, *J* = 2, *J* = 4); 7.22 (d, 1H, *J* = 4); 7.93 (d, 1H, *J* = 2); 8.65 (bs, 1H); 8.77 (s, 1H); 9.01 (bs, 1H). Anal. (C₂₄H₃₄N₈O₂) C, H, N.

4-[3-(2-Furan-2-yl-8-*n*-octyl-8*H*-pyrazolo[4,3-*e*]1,2,4-triazolo[1,5-*c*]pyrimidin-5-yl)ureido]phenylacetic Acid Ethyl Ester (118). Yield: 87%; white solid. IR (KBr): 3240–2950, 1730, 1665, 1615, 1600, 1530 cm⁻¹. ¹H NMR (CDCl₃) δ: 0.86 (t, 3H, *J* = 7); 1.09–1.31 (m, 13H); 1.97–2.11 (m, 2H); 3.56 (s, 1H); 4.15 (q, 2H, *J* = 7); 4.36 (t, 2H, *J* = 7); 6.62 (dd, 1H, *J* = 2, *J* = 4); 7.19 (d, 2H, *J* = 9); 7.23 (d, 1H, *J* = 4); 7.62 (d, 2H, *J* = 7); 7.64 (d, 1H, *J* = 2); 8.21 (s, 1H); 8.57 (bs, 1H); 11.13 (bs, 1H). Anal. (C₂₉H₃₄N₈O₄) C, H, N.

5-[[4-Tolyl]amino]carbonylamino-8-*n*-octyl-2-(2-furyl)pyrazolo[4,3-*e*]1,2,4-triazolo[1,5-*c*]pyrimidine (119). Yield: 77%; white solid. IR (KBr): 3230–2940, 1675, 1615, 1580 cm⁻¹. ¹H NMR (CDCl₃) δ: 0.84 (t, 3H, *J* = 7); 1.09–1.21 (m, 10H); 1.95–2.05 (m, 2H); 2.31 (s, 3H); 4.36 (t, 2H, *J* = 7); 6.60 (dd, 1H, *J* = 2, *J* = 4); 7.15 (d, 2H, *J* = 9); 7.23 (d, 1H, *J* = 4); 7.55 (d, 2H, *J* = 9); 7.64 (d, 1H, *J* = 2); 8.20 (s, 1H); 8.56 (bs, 1H); 11.02 (bs, 1H). Anal. (C₂₆H₃₀N₈O₂) C, H, N.

5-[[Cyclohexyl]amino]carbonylamino-8-cyclohexylmethyl-2-(2-furyl)pyrazolo[4,3-*e*]1,2,4-triazolo[1,5-*c*]pyrimidine (120). Yield: 74%; white solid. IR (KBr): 3245–2935, 1672, 1610, 1560 cm⁻¹. ¹H NMR (CDCl₃) δ: 0.93–2.01 (m, 21H); 3.48–3.56 (m, 1H); 4.19 (d, 2H, *J* = 6); 6.78 (dd, 1H, *J* = 2, *J* = 4); 7.22 (d, 1H, *J* = 4); 7.98 (d, 1H, *J* = 2); 8.63 (bs, 1H); 8.76 (s, 1H); 8.98 (bs, 1H). Anal. (C₂₄H₃₀N₈O₂) C, H, N.

5-[[*n*-Pentyl]amino]carbonylamino-8-*n*-octyl-2-(2-furyl)pyrazolo[4,3-*e*]1,2,4-triazolo[1,5-*c*]pyrimidine (121). Yield: 83%; white solid. IR (KBr): 3245–2965, 1665, 1615,

1550 cm^{-1} . ^1H NMR (CDCl_3) δ : 0.82–1.97 (m, 22H); 4.11 (d, 2H, $J = 6$); 6.72 (dd, 1H, $J = 2$, $J = 4$); 7.25 (d, 1H, $J = 4$); 7.94 (d, 1H, $J = 2$); 8.73 (bs, 1H); 8.75 (s, 1H); 8.97 (bs, 1H). Anal. ($\text{C}_{23}\text{H}_{30}\text{N}_8\text{O}_2$) C, H, N.

4-[3-(2-Furan-2-yl-8-cyclohexylmethyl-8*H*-pyrazolo[4,3-*e*][1,2,4]triazolo[1,5-*c*]pyrimidin-5-yl)ureido]phenylacetic Acid Ethyl Ester (122). Yield: 69%; white solid. IR (KBr): 3255–2966, 1725, 1670, 1625, 1600, 1510 cm^{-1} . ^1H NMR (CDCl_3) δ : 1.20 (t, 3H, $J = 7$); 1.41–1.92 (m, 11H); 3.59 (s, 1H); 4.12 (d, 2H, $J = 6$); 4.16 (q, 2H, $J = 7$); 6.61 (dd, 1H, $J = 2$, $J = 4$); 7.21 (d, 2H, $J = 9$); 7.24 (d, 1H, $J = 4$); 7.61 (d, 2H, $J = 7$); 7.63 (d, 1H, $J = 2$); 8.17 (s, 1H); 8.59 (bs, 1H); 11.15 (bs, 1H). Anal. ($\text{C}_{28}\text{H}_{30}\text{N}_8\text{O}_4$) C, H, N.

5-[(4-Tolyl)amino]carbonylamino-8-cyclohexylmethyl-2-(2-furyl)pyrazolo[4,3-*e*]1,2,4-triazolo[1,5-*c*]pyrimidine (123). Yield: 87%; white solid. IR (KBr): 3250–2955, 1673, 1620, 1570 cm^{-1} . ^1H NMR (CDCl_3) δ : 0.93–1.21 (m, 6H); 1.42–1.78 (m, 4H); 1.97–2.12 (m, 1H); 2.29 (s, 3H); 4.15 (d, 2H, $J = 6$); 6.59 (dd, 1H, $J = 2$, $J = 4$); 7.18 (d, 2H, $J = 9$); 7.24 (d, 1H, $J = 4$); 7.51 (d, 2H, $J = 9$); 7.64 (d, 1H, $J = 2$); 8.16 (s, 1H); 8.56 (bs, 1H); 11.00 (bs, 1H). Anal. ($\text{C}_{25}\text{H}_{26}\text{N}_8\text{O}_2$) C, H, N.

Appendix

Abbreviations. CGS15943, 5-amino-9-chloro-2-(2-furyl)[1,2,4]triazolo[1,5-*c*]quinazoline; MRS1220, 9-chloro-2-(2-furyl)-[1,2,4]triazolo[1,5-*c*]quinazoline; CHA, N^6 -cyclohexyladenosine; DPCPX, 1,3-dipropyl-8-cyclopentylxanthine; DMSO, dimethyl sulfoxide; THF, tetrahydrofuran; CHO cells, chinese Hamstery ovary cells; EDTA, ethylenediaminetetraacetate; SCH58261, 5-amino-2-(2-furyl)-7-(2-phenylethyl)pyrazolo[4,3-*e*][1,2,4]triazolo[1,5-*c*]pyrimidine; IB-MECA, 3-iodobenzyl-5'-(*N*-ethylcarbamoyl)adenosine; NECA, 5'-(*N*-ethylcarbamoyl)adenosine; HEK cells, human embryonic kidney cells; MRE3008-F20, 5-[(4-methoxyphenyl)amino]carbonylamino-8-propyl-2-(2-furyl)pyrazolo[4,3-*e*]1,2,4-triazolo[1,5-*c*]pyrimidine; GTP, guanosine 5'-triphosphate; cAMP, cyclic adenosine 5'-monophosphate; ATP, adenosine 5'-triphosphate; TLC, thin-layer chromatography; HCl, hydrochloric acid; mp, melting point; EtOAc, ethyl acetate; HPLC, high performance liquid chromatography; IR, infrared spectra; NMR, nuclear magnetic resonance; CDCl_3 , deuterated chloroform; 3D-QSAR, three-dimensional quantitative structure–activity relationship; CoMFA, comparative molecular field analysis; PLS, partial least squares; QSAR, quantitative structure–activity relationship; r^2_{bs} , correlation coefficient from bootstrap analysis; r^2_{cv} , correlation coefficient from cross-validation equation; rms, root mean square; GPCR, G protein-coupled receptor.

Acknowledgment. The molecular modeling work coordinated by S.M. has been carried out with financial support of Associazione Italiana per la Ricerca sul Cancro (AIRC), Milan, and the Italian Ministry for University and Research (MIUR), Rome, Italy. S.M. is strongly grateful to Christian Montopoli and Andrea Tralli for the scientific collaboration in developing the human A_3 receptor model. S.M. is also really grateful to Chemical Computing Group for the scientific and technical partnership.

Supporting Information Available: Tables listing actual vs predicted CoMFA results and elemental analyses of compounds 11–60 and 65–68. This material is available free of charge via the Internet at <http://pubs.acs.org>.

References

- Fredholm, B. B.; Arslan, G.; Halldner, L.; Kull, B.; Schulte, G.; et al. Structure and function of adenosine receptors and their genes. *Naunyn-Schmiedeberg's Arch. Pharmacol.* **2000**, *362*, 364–374.
- Merighi, S.; Mirandola, P.; Varani, K.; Gessi, S.; Leung, E.; et al. A glance at adenosine receptors: novel target for antitumor therapy. *Pharmacol. Ther.* **2003**, *100*, 31–48.
- Rorke, S.; Holgate, S. T. Targeting adenosine receptors: novel therapeutic targets in asthma and chronic obstructive pulmonary disease. *Am. J. Respir. Med.* **2002**, *1*, 99–105.
- Guimaraes, S.; Morato, M.; Sousa, T.; Albino-Teixeira, A. Hypertension due to blockade of adenosine receptors. *Pharmacol. Toxicol.* **2003**, *92*, 160–162.
- Blum, D.; Hourez, R.; Galas, M. C.; Popoli, P.; Schiffmann, S. N. Adenosine receptors and Huntington's disease: implications for pathogenesis and therapeutics. *Lancet Neurol.* **2003**, *2*, 366–374.
- Moreau, J. L.; Huber, G. Central adenosine A_{2A} receptors: an overview. *Brain Res. Brain Res. Rev.* **1999**, *31*, 65–82.
- Haas, H. L.; Selbach, O. Functions of neuronal adenosine receptors. *Naunyn-Schmiedeberg's Arch. Pharmacol.* **2000**, *362*, 375–381.
- von Lubitz, D. K.; Ye, W.; McClellan, J.; Lin, R. C. Stimulation of adenosine A_3 receptors in cerebral ischemia. Neuronal death, recovery, or both? *Ann. N.Y. Acad. Sci.* **1999**, *890*, 93–106.
- Shryock, J. C.; Belardinelli, L. Adenosine and adenosine receptors in the cardiovascular system: biochemistry, physiology, and pharmacology. *Am. J. Cardiol.* **1997**, *79*, 2–10.
- Jacobson, K. A. Adenosine A_3 receptors: novel ligands and paradoxical effects. *Trends Pharmacol. Sci.* **1998**, *19*, 184–191.
- Olah, M. E.; Ren, H.; Stiles, G. L. Adenosine receptors: protein and gene structure. *Arch. Int. Pharmacodyn. Ther.* **1995**, *329*, 135–150.
- Linden, J. Cloned adenosine A_3 receptors: pharmacological properties, species differences and receptor functions. *Trends Pharmacol. Sci.* **1994**, *15*, 298–306.
- Jacobson, K. A.; Moro, S.; Manthey, J. A.; West, P. L.; Ji, X. D. Interactions of flavones and other phytochemicals with adenosine receptors. *Adv. Exp. Med. Biol.* **2002**, *505*, 163–171.
- Baraldi, P. G.; Cacciari, B.; Romagnoli, R.; Merighi, S.; Varani, K.; et al. A_3 adenosine receptor ligands: history and perspectives. *Med. Res. Rev.* **2000**, *20*, 103–128.
- Baraldi, P. G.; Cacciari, B.; Moro, S.; Spalluto, G.; Pastorin, G.; et al. Synthesis, biological activity, and molecular modeling investigation of new pyrazolo[4,3-*e*]-1,2,4-triazolo[1,5-*c*]pyrimidine derivatives as human A_3 adenosine receptor antagonists. *J. Med. Chem.* **2002**, *45*, 770–780.
- Baraldi, P. G.; Cacciari, B.; Spalluto, G.; Bergonzoni, M.; Dionisotti, S.; et al. Design, synthesis, and biological evaluation of a second generation of pyrazolo[4,3-*e*]-1,2,4-triazolo[1,5-*c*]pyrimidines as potent and selective A_{2A} adenosine receptor antagonists. *J. Med. Chem.* **1998**, *41*, 2126–2133.
- Baraldi, P. G.; Cacciari, B.; Romagnoli, R.; Spalluto, G.; Klotz, K. N.; et al. Pyrazolo[4,3-*e*]-1,2,4-triazolo[1,5-*c*]pyrimidine derivatives as highly potent and selective human A_3 adenosine receptor antagonists. *J. Med. Chem.* **1999**, *42*, 4473–4478.
- Baraldi, P. G.; Cacciari, B.; Romagnoli, R.; Spalluto, G.; Moro, S.; et al. Pyrazolo[4,3-*e*]1,2,4-triazolo[1,5-*c*]pyrimidine derivatives as highly potent and selective human A_3 adenosine receptor antagonists: influence of the chain at the N(8) pyrazole nitrogen. *J. Med. Chem.* **2000**, *43*, 4768–4780.
- Baraldi, P. G.; Cacciari, B.; Borean, P. A.; Varanin, K.; Pastorin, G.; et al. Pyrazolo-triazolo-pyrimidine derivatives as adenosine receptor antagonists: a possible template for adenosine receptor subtypes? *Curr. Pharm. Des.* **2002**, *8*, 2299–2332.
- Pastorin, G.; Da Ros, T.; Spalluto, G.; Deflorian, F.; Moro, S.; et al. Pyrazolo[4,3-*e*]-1,2,4-triazolo[1,5-*c*]pyrimidine derivatives as adenosine receptor antagonists. Influence of the N5 substituent on the affinity at the human A_3 and A_{2B} adenosine receptor subtypes: a molecular modeling investigation. *J. Med. Chem.* **2003**, *46*, 4287–4296.
- Wang, R.; Lu, Y.; Wang, S. Comparative evaluation of 11 scoring functions for molecular docking. *J. Med. Chem.* **2003**, *46*, 2287–2303.
- Clark, R. D.; Strizhev, A.; Leonard, J. M.; Blake, J. F.; Matthew, J. B. Consensus scoring for ligand/protein interactions. *J. Mol. Graphics Modell.* **2002**, *20*, 281–295.
- Bissantz, C.; Folkers, G.; Rognan, D. Protein-based virtual screening of chemical databases. 1. Evaluation of different docking/scoring combinations. *J. Med. Chem.* **2000**, *43*, 4759–4767.
- Chen, Y. Z.; Gu, X. L.; Cao, Z. W. Can an optimization/scoring procedure in ligand-protein docking be employed to probe drug-resistant mutations in proteins? *J. Mol. Graphics Modell.* **2001**, *19*, 560–570.

- (25) Moro, S.; Deflorian, F.; Spalluto, G.; Pastorin, G.; Cacciari, B.; et al. Demystifying the three-dimensional structure of G protein-coupled receptors (GPCRs) with the aid of molecular modeling. *Chem. Commun. (Cambridge)* **2003**, 2949–2956.
- (26) Maconi, A.; Pastorin, G.; Da Ros, T.; Spalluto, G.; Gao, Z. G.; et al. Synthesis, biological properties, and molecular modeling investigation of the first potent, selective, and water-soluble human A₃ adenosine receptor antagonist. *J. Med. Chem.* **2002**, *45*, 3579–3582.
- (27) Palczewski, K.; Kumasaka, T.; Hori, T.; Behnke, C. A.; Motoshima, H.; et al. Crystal structure of rhodopsin: A G protein-coupled receptor. *Science* **2000**, *289*, 739–745.
- (28) Olah, M. E.; Jacobson, K. A.; Stiles, G. L. Role of the second extracellular loop of adenosine receptors in agonist and antagonist binding. Analysis of chimeric A₁/A₃ adenosine receptors. *J. Biol. Chem.* **1994**, *269*, 24692–24698.
- (29) Gao, Z. G.; Van Muijlwijk-Koezen, J. E.; Chen, A.; Muller, C. E.; Ijzerman, A. P.; et al. Allosteric modulation of A₃ adenosine receptors by a series of 3-(2-pyridinyl)isoquinoline derivatives. *Mol. Pharmacol.* **2001**, *60*, 1057–1063.
- (30) Gao, Z. G.; Chen, A.; Barak, D.; Kim, S. K.; Muller, C. E.; et al. Identification by site-directed mutagenesis of residues involved in ligand recognition and activation of the human A₃ adenosine receptor. *J. Biol. Chem.* **2002**, *277*, 19056–19063.
- (31) Jiang, Q.; Lee, B. X.; Glashofer, M.; van Rhee, A. M.; Jacobson, K. A. Mutagenesis reveals structure–activity parallels between human A_{2A} adenosine receptors and biogenic amine G protein-coupled receptors. *J. Med. Chem.* **1997**, *40*, 2588–2595.
- (32) Jiang, Q.; Van Rhee, A. M.; Kim, J.; Yehle, S.; Wess, J.; et al. Hydrophilic side chains in the third and seventh transmembrane helical domains of human A_{2A} adenosine receptors are required for ligand recognition. *Mol. Pharmacol.* **1996**, *50*, 512–521.
- (33) OpenMosix, <http://www.openMosix.org>, 2004.
- (34) Molecular Operating Environment (MOE 2003.02), C.C.G., Inc., 1255 University St., Suite 1600, Montreal, Quebec, Canada, H3B 3X3.
- (35) SYBYL TRIPOS Associates, St. Louis, MO, 1993, version 6.5.
- (36) MOPAC available from Quantum Chemistry Program Exchange, version 6.0.
- (37) Saunders: J. Rhodopsin crystal structure: provides information on GPCR-ligand binding in general? *Drug Discovery Today* **2001**, *6*, 288–289.
- (38) Cornell, W. D. C. P.; Bayly, C. I.; Gould, I. R.; Merz, K. M.; Ferguson, D. M.; Spellmeyer, D. C.; Fox, T.; Caldwell, J. W.; Kollman, P. A. A Second Generation Force Field for the Simulation of Proteins, Nucleic Acids and Organic Molecules. *J. Am. Chem. Soc.* **1995**, *117*, 5179–5196.
- (39) Baxter, C. A.; Murray, C. W.; Clark, D. E.; Westhead, D. R.; Eldridge, M. D. Flexible Docking Using Tabu Search and an Empirical Estimate of Binding Affinity. *Proteins: Struct., Funct., Genet.* **1998**, *33*, 367–382.
- (40) Halgren, T. Merck Molecular Force Field. I. Basis, Form, Scope, Parameterization, and Performance of MMFF94. *J. Comput. Chem.* **1996**, *17*, 490–519.
- (41) Varani, K. G. S.; Dionisotti, S.; Ongini, E.; Borea, P. A. [3H]-SCH 58261 Labelling of functional A_{2A} adenosine receptors in human neutrophil membranes. *Br. J. Pharmacol.* **1998**, *123*, 1723–1731.
- (42) Bradford, M. M. A rapid sensitive method for the quantification of microgram quantities of protein utilizing the principle of protein dye-binding. *Anal. Biochem.* **1976**, *72*, 248–254.
- (43) Wold, S. R. A.; Wold, H.; Dunn, W. J. The Covariance Problem in Linear Regression. The Partial Least Squares (PLS) Approach to Generalized Inverses. *SIAM J. Sci. Stat. Comput.* **1994**, *5*, 735–743.
- (44) Cramer, R. D., III; Bunce, J. D.; Patterson, D. E.; Frank, I. E. Crossvalidation, Bootstrapping, and Partial Least Squares Compared with Multiple Regression in Conventional QSAR Studies. *Quant. Struct.-Act. Relat.* **1988**, *7*, 18–25.
- (45) Waller, C. L.; Oprea, T. I.; Giolitti, A.; Marshall, G. R. Three-Dimensional QSAR of Human Immunodeficiency Virus (I) Protease Inhibitors. 1. A CoMFA Study Employing Experimentally-Determined Alignment Rules. *J. Med. Chem.* **1993**, *36*, 4152–4160.

JM049662F